Journal of the Serbian Chemical Society
JSCS-info@shd.org.rs • www.shd.org.rs/JSCS
J. Serb. Chem. Soc. 90 (10) 1223–1239 (2025)
JSCS–5450
Original scientific paper
Published 26 October, 2025

Synthesis of zeolite LTA from kaolin and its model CBC and WAC performance: Optimized by central composite design

GÜL AKAR ŞEN*

Dokuz Eylul University, Faculty of Engineering, Mining Engineering Department, İzmir, Turkiye

(Received 10 March, revised 8 April, accepted 22 July 2025)

Abstract: In this study, a cost-effective route to synthesizing LTA-type zeolite from Balıkesir-region kaolin was demonstrated. Kaolin was calcined at 800 °C to obtain metakaolin, which was then treated hydrothermally in the presence of NaOH under optimized conditions determined by a Box–Behnken experimental design. The process variables NaOH concentration, temperature, and solid to liquid ratio were systematically investigated to maximize both water adsorption capacity and cation-exchange capacity (*CEC*). Quadratic regression models and ANOVA confirmed that NaOH concentration and temperature exert the most significant impact on zeolite formation and performance. Characterization by XRD, SEM and FTIR confirmed that the synthesized product under optimal conditions predominantly consisted of LTA-type zeolite crystals, as evidenced by the characteristic diffraction peaks, morphology and vibrational bands. The best performing sample showed a *CEC* of up to 192 mg $CaCO_3$ g^{-1} and a water adsorption capacity of nearly 29 g H_2O per 100 g adsorbent. These results highlight the potential of locally sourced kaolin for producing high value zeolites, offering a sustainable alternative to imported raw materials.

Keywords: synthesis of zeolite; zeolite LTA; kaolin; hydrothermal synthesis; ANOVA.

INTRODUCTION

Rapid urbanization and industrial growth have significantly increased environmental pollution, especially due to industrial waste disposal.[1] Energy-intensive industries notably contribute to environmental degradation.[2,3] Zeolites, owing to their interconnected micro and mesoporous framework that confers highly selective adsorption and ion-exchange behavior, play a pivotal role in industrial separations, environmental remediation and heterogeneous catalysis. They are crystalline aluminosilicates formed by tetrahedral units of silicon, aluminum and oxygen,

* Correspondence E-mail: gul.akar@deu.edu.tr
https://doi.org/10.2298/JSC250310054A

where the negative charge from Al is balanced by cations (Na^+, K^+, Ca^{2+}).[4–8] Their adsorption capacity,[9] molecular sieving, and ion-exchange properties make zeolites valuable in various applications,[9–12] including hydrocarbon separation, heavy metal removal, water softening through ammonium removal by ion-exchange,[13,14] and catalysis/sensor supports.[15]

Both natural and synthetic zeolites contain aluminosilicates incorporating elements from groups I and II. According to the International Zeolite Association Structure Commission, more than 260 unique zeolite framework types have now been officially approved and assigned three-letter codes.[16] Synthetic zeolites have been produced through microwave, vapor, and hydrothermal methods from diverse silica/alumina sources.[17–21] Among materials explored (kaolin, clay, fly ash, feldspar, bauxite), kaolin is highlighted for its economic viability and high silica/alumina content, making it an ideal precursor for synthesizing LTA-type zeolites.[22,23] The synthesis involves converting kaolin into reactive metakaolin by calcination, followed by hydrothermal crystallization. Important parameters include silica-to-alumina ratio, reaction time, temperature, hydrodynamics and pH. Due to their uniform pore size, crystallinity, and robust structure, LTA-type zeolites (such as zeolite 4A) are widely utilized in ion-exchange, adsorption and catalysis.[24]

Turkey imports a variety of synthetic zeolites: around fifty thousand tons per year for detergents, ten thousand tons per year for insulating glass applications, and approximately five thousand tons annually for use as petrochemical catalysts. Local production is minimal, primarily due to higher production costs linked to imported raw materials. The main goal of this study is to synthesize zeolite 4A (LTA) from locally available Turkish kaolin, which may differ from international sources. Previous research on synthesizing zeolites from kaolin has focused on optimizing the process for environmental applications, such as pollutant removal.[25–27] In line with this, the present work aims to synthesize LTA-type zeolites from Balıkesir-region kaolin and optimize their cation exchange capacity (*CEC*) and water adsorption capacity using response surface methodology (RSM). A central composite design (CCD) was employed to identify the best set of synthesis conditions, and the resulting materials were characterized extensively, including structural and adsorption properties.

EXPERIMENTAL

Materials and methods

A Balıkesir-region kaolin (K) was used as the starting material. Wet chemical analyses in aqua regia were performed using an Analytik Jena NovaA 300 AAS to determine the oxide compositions of the samples. The raw sample is labeled “K”. To remove impurities, the raw material was treated with sodium dithionite ($Na_2S_2O_4$) at a concentration of 0.3 g per 100 g of kaolin (pH adjusted to 3 with H_2SO_4).[28] The treated kaolin is labeled “TK”. After drying and sieving, synthetic zeolite LTA was obtained from TK, which was first converted to metakaolin (MK) by calcination at 800 °C for 2 h, followed by hydrothermal synthesis. Particle size distri-

butions (volume based D_{80}) were measured with a Horiba LA-950 V2 laser diffraction analyser. Samples were dispersed in isopropanol and ultrasonicated for 2 min at 40 W prior to measurement to ensure uniform particle dispersion. Specific gravity was determined with a Micromeritics AccuPyc II 1340 helium gas pycnometer (five measurement cycles; precision ±0.002 g cm^{-3}). Hardness was assessed on pelletised specimens using a Vickers micro-hardness tester (Shimadzu HMV-2), reported as average of five indents. pH measured on a 10 wt. % solid suspension with a pH meter (calibrated at 25 °C with NBS buffers 4.00/7.00). Elemental composition of major oxides determined by flame AAS (Analytik Jena novAA 300) and expressed on an LOI-free basis. X-ray diffraction (XRD) analyses were performed on a Rigaku Miniflex II diffractometer with CuKα radiation (30 kV, 15 mA, 2θ range: 3–55°). Morphological studies were conducted using a Jeol JXA-733 Superprobe SEM. FT-IR analyses of selected products used a Perkin Elmer Spectrum BX in the range of 500–4000 cm^{-1} with 4 cm^{-1} resolutions. All chemicals ($Na_2S_2O_4$, NaOH, HCl and H_2SO_4) were Sigma–Aldrich grade and used without further purification. Deionized water was produced via a Millipore Milli-Q system.

Calcination (metakaolinization)

Calcination is critical in transforming kaolin into metakaolin by destroying the layered kaolinite lattice.[24,29] This process typically occurs at 600–900 °C. The transition starts near 600 °C, and near 800 °C, kaolin is mostly converted into an amorphous metakaolin.[31] Optimization of temperature and duration depends on the raw material's quality, which in turn depends on mining sites.[24] In this work, TK was calcined in a muffle furnace at a heating rate of 3 °C/min up to 800 °C, held for 2 h, then cooled naturally. The product is labelled MK.

Synthesis of zeolite LTA using central composite experimental design

Zeolite LTA was synthesized from TK-derived metakaolin under hydrothermal conditions. Based on literature findings that crystallinity increases significantly after 3–4 h, a reaction time of 24 h was chosen. Temperatures below 50 °C were deemed unsuitable for crystallization.[24,28-33] Temperature, NaOH concentration and solid-to-liquid (S/L) ratio, known to affect crystallization, were selected as the experimental variables in a Box–Behnken design (BBD) combined with RSM. BBD allows the sequential examination of parameters while keeping others constant.[34] The selected variables and their levels, as shown in Table I, were defined as follows: NaOH concentration (2, 2.5 and 3 M), solid-to-liquid ratio (20, 25 and 30 %) and temperature (60, 75 and 90 °C).

TABLE I. Box–Behnken design parameters and experimental conditions; –1: factor at low level; 0: factor at medium level; +1: factor at high level

Variable	Symbol	–1	0	+1
NaOH (mol/L as M)	A	2	2.5	3
Temperature, °C	B	60	75	90
Solid/liquid ratio, %	C	20	25	30

A key advantage of the BBD with RSM methodology is its ability to analyse multiple parameters with fewer experimental trials compared to other methods.[34] In this study, three factors at three levels (low, medium and high) were evaluated, represented by –1, 0 and +1, respectively. The test variables were designated as NaOH concentration (A), temperature (B), and solid-to-liquid ratio (C), while the responses, water adsorption (Y_1) and cation exchange capacity (CEC, Y_2), were investigated.

The second-order polynomial equation was used to predict the relationship between the independent variables and the response, as represented by:

$$Y_{1,2} = b_0 + b_1A + b_2B + b_3C + b_{12}AB + b_{13}AC + b_{23}BC + b_{11}A^2 + b_{22}B^2 + b_{33}C^2 \quad (1)$$

where Y is the predicted response, b_0 is the constant term, A, B, C are the independent variables, b_1, b_2, b_3 are linear coefficients, b_{12}, b_{13}, b_{23} are interaction coefficients, and b_{11}, b_{22}, b_{33} are quadratic coefficients. ANOVA and 3D surface plots (Stat-Ease 360 software) were used to determine model fit and analyse parameter interactions.

Following the experimental design, 5.0 g of metakaolin was mixed with NaOH at the specified *S*/*L* ratios and stirred at 250 rpm for 24 h. The resulting gel was subjected to hydrothermal synthesis at different temperatures. After the reaction, the gel was washed until reaching pH 9––10, filtered, and dried at 100 °C for 12 h. The synthesis route is summarized in Fig. 1.

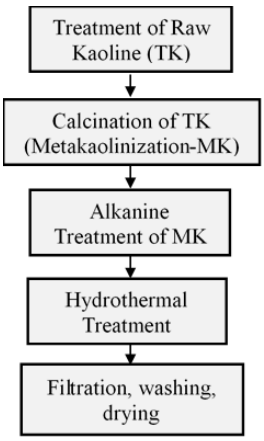

Fig 1. Schematic representation of hydrothermal synthesis procedure of zeolites.

*Cation-exchange capacity (*CEC*) and water adsorption amounts*

Cation-exchange capacity (*CEC*) was determined by Ca^{2+} exchange following Hui & Chao (2006) with minor modifications.[21] Precisely 0.100±0.001 g of each sample (pre-dried at 105 °C for 2 h) was contacted with 50.0 mL of 0.010 M $CaCl_2$ in a 100 mL polyethylene conical flask. Suspensions were agitated in an orbital shaker (IKA KS-4000) at 25±0.2 °C, 150 rpm for 24 h. Supernatants were centrifuged (10 min) and filtered (0.45 μm nylon); Ca^{2+} was analysed with a PCa-1-01 ion selective electrode calibrated from 0.5×10^{-3} to 5×10^{-3} M:

$$CEC = 100.08V(C_0 - C_1)/m \quad (2)$$

where *CEC* represents the calcium ion-exchange capacity of the product (mg $CaCO_3$ g^{-1}), 100.08 is the molar mass of $CaCO_3$ (g/mol or mg/mmol), C_0 is the initial Ca^{2+} concentration in the $CaCl_2$ solution (mol/L), C_1 is the Ca^{2+} concentration in the filtrate (mol/L), V is the volume of the $CaCl_2$ solution (mL), and m is the mass of the sample (g).

For water-adsorption tests the exchanged solids were re-dried at 60 °C for 24 h, then placed in a Binder KBF 115 climate chamber at 25±0.3 °C, 68±0.2 % RH with 0.3 m s^{-1} airflow. Mass gain after 24 h was recorded and expressed as g H_2O per 100 g adsorbent. This method allows for the quantification of the water adsorption amounts of the synthesized zeolites, providing insight into their potential applications in moisture-sensitive environments.

RESULTS AND DISCUSSION

Physical and chemical characterization

Raw Balıkesir kaolin was crushed, ground below 106 μm, and analyzed for specific gravity, hardness, pH and particle size. Table II shows that metakaolin (MK) had increased density and hardness, and reduced particle size compared to treated kaolin (TK), primarily due to removal of structurally bound water. During calcination at 800 °C, the dehydroxylation of kaolinite removes structural –OH groups, leading to the collapse of the layered lattice into an amorphous, highly brittle metakaolin. This structural collapse, combined with the release of interlayer water, weakens inter-particle cohesion and promotes fragmentation.[35] Consequently, even mild grinding and dispersion steps after calcination generate much finer platelets, which accounts for the observed D_{80} drop from 102.15 (TK) to 3.65 μm (MK).

TABLE II. Some physical properties of TK and MK samples

Samples	Specific gravity, g/cm^3	Hardness	pH	Particle size, D_{80} / μm
TK	2.609	1.72	6.91	102.15
MK	2.615	6.22	6.91	3.65

Wet chemical analyses were conducted using an Analytik Jena NovaA 300 atomic absorption spectrometer (AAS) to determine the concentration of applicable elements in the final solutions. The chemical composition of T, TK and MK are shown in Table III

TABLE III. Chemical composition of samples kaoline (K)and treated kaoline (TK); *LOI* = loss on ignition

Sample	SiO_2	Al_2O_3	Fe_2O_3	CaO	MgO	Na_2O	K_2O	TiO_2	MnO	*LOI*
Kaoline (K)	51.37	36.95	0.45	0.43	0.11	0.01	0.34	0.47	0.01	9.12
Treated Kaoline (TK)	52.18	37.68	0.11	0.22	0.08	0.01	0.14	0.24	0.01	8.18
Metakaoline (MK)	58.38	38.95	0.10	0.19	0.11	0.08	0.12	0.23	0.01	1.06

The Si/Al mole ratio of MK was 1.50, which is within the typical range (1.0––1.8) associated with the formation of low-silica zeolite frameworks such as LTA and sodalite. While the synthesis mixture can accommodate a broader range, this ratio in the final product is often considered favorable for achieving high LTA crystallinity.[36,37]

Mineralogical and morphological characterization of TK and MK

The XRD pattern of TK and MK is shown in Fig. 2. The XRD pattern of treated kaolin exhibits the diagnostic basal reflections of kaolinite at $2\theta \approx 12.3°$ (*d001* ≈ 7.15 Å) and 24.9° (*d002* ≈ 3.57 Å), assigned to the (001) and (002) planes,

confirming the layered kaolinite structure.[31] Upon a single calcination step at 800 °C for 2 h, the XRD patterns exhibit the expected significant change in comparison to the pattern of TK, the characteristic kaolinite peaks at 2θ ~ 12.3° (001) and ~24.9° (002) disappear, and the diffractogram develops a broad hump centred at ~25°, consistent with the formation of largely amorphous metakaolin which was characterized by the disappearance of the diffraction peaks of kaolinite, accompanied by the appearance of amorphous aluminosilicate (Fig. 2). These findings are consistent with the related literature.[31]

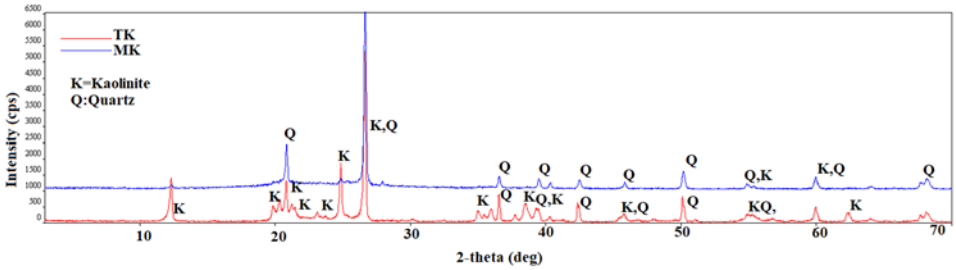

Fig. 2. XRD pattern of treated kaolin (TK) and metakaoline (MK).

SEM analyses were carried out to assess the samples' morphological features. In Fig. 3a, the typical layered, plate-like structure of kaolinite is evident. However, after calcination (Fig. 3b), this layered structure was lost, and particle size was notably reduced, leaving behind an irregular, disorganized plate morphology. Calcination promotes the dehydroxylation of kaolinite, altering the local environment of the aluminum atoms as they transition from octahedral to tetrahedral coordination. As a result, the material becomes amorphous and more reactive.[38]

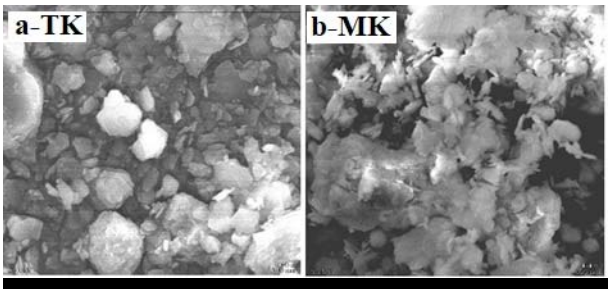

Fig 3. SEM pictures of treated kaolin (TK) and metakaoline (MK).

Results of synthesis of zeolite LTA using Box–Behnken design with RSM methodology

Seventeen experimental runs and three control trials were carried out to evaluate the effects of the three variables. The actual data obtained from these tests

were utilized to derive mathematical equations describing how the independent variables influence the *CEC* and water adsorption capacity of the synthesized LTA. Table IV presents the conditions of the design matrix, along with the corresponding experimental outcomes. Notably, the experimental program produced an LTA sample with a *CEC* of up to 186.82 mg $CaCO_3$ g^{-1} and a water adsorption capacity of 29.09 g H_2O per 100 g of adsorbent.

TABLE IV. BBD with RSM designed experimental results

Run	Factor 1 *A*: NaOH (mol/L)	Factor 2 *B*: Temperature °C	Factor 3 *C*: *S*/*L* ratio %	Response 1 Water absorbed, g H_2O/100 g adsorbent		Response 2 *CEC* mg $CaCO_3$ g^{-1}	
				Actual	Predicted	Actual	Predicted
1	2	60	25	25.45	25.29	142.25	142.84
2	2.5	60	20	26.65	26.75	170.91	171.56
3	2.5	60	30	26.52	26.56	168.53	167.10
4	3	60	25	26.91	26.88	175.41	175.39
5	2	75	20	26.35	26.39	155.34	154.05
6	2	75	30	26.21	26.31	149.98	150.81
7	2.5	75	25	29.08	29.03	185.03	185.79
8	2.5	75	25	29.06	29.03	186.55	185.72
9	2.5	75	25	29.05	29.03	185.96	185.79
10	2.5	75	25	29.09	29.04	186.82	185.79
11	2.5	75	25	28.87	29.03	184.61	185.79
12	3	75	20	27.75	27.66	185.19	184.36
13	3	75	30	27.23	27.17	182.52	183.82
14	2	90	25	27.78	27.81	165.39	165.45
15	2.5	90	20	28.92	28.85	188.91	190.34
16	2.5	90	30	28.53	28.43	191.78	191.07
17	3	90	25	28.15	28.31	192.43	192.84

Fig. 4 shows the solid linear relationship between the experimental and predicted values of the responses. The determination coefficients R^2 of 0.9940 and 0.9963 of the water adsorbed amounts (g H_2O/100 g^{-1}) and *CEC* (mg $CaCO_3$ g^{-1}), respectively, shows that the fit is reasonably good. The actual and predicted values of both the water adsorbed amounts and *CEC* obtained using model equations are presented in Fig. 4a and b. The predicted values are in good agreement with the experimental values.

Table V shows the analysis of variance of the developed models for the *CEC* and water adsorption amounts of synthesized zeolite LTA. Fisher's test with corresponding (*P*) values was used to study the effect of different parameters on two responses on the result of analysis by ANOVA analysis model. The models are significant as the *F* value is high, the *Prob*>*F* value is less than 0.05 and the standard deviation is very small: 0.14 for the water adsorption amounts and 1.42 for the *CEC*:

$$Y_1 = 28.64 + 0.6208A + 0.9189B - 0.1258C - 0.1867AB - 0.0950AC - \\ -0.0433BC - -1.36A^2 - 0.2622B^2 - 0.7850C^2 \quad (3)$$

$$Y_2 = 182.00 + 16.00A + 8.04B - 1.38C - 0.3533AB + 0.6725AC - \\ -0.8750BC - 13.85A^2 - 0.9220B^2 - 3.69C^2 \quad (4)$$

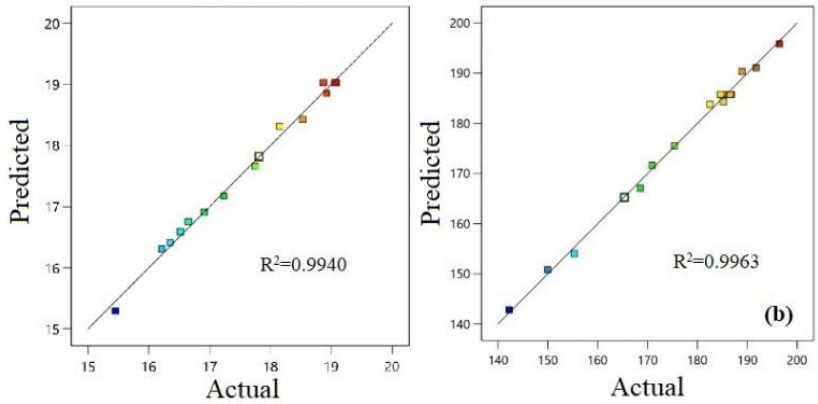

Fig. 4. Relationship between observed and predicted values (a: water adsorbed amounts, b: *CEC*).

TABLE V. ANOVA for the parameters of RSM-BBD

Statistics	Water absorbed g H_2O/100 g adsorbent	*CEC* / mg $CaCO_3$ g^{-1}
Sum of square	23.54	3861.23
Degree of freedom	9	9
Mean square	2.62	429.03
F-Value	129.60	211.80
Prob>F	<0.0001	<0.0001
Standard deviation	0.14	1.42
R^2	0.9940	0.9963
Lack of fit (*p*-values)	0.093	0.112

The model *F*-value of 129.60 indicates that the model is significant for Response 1 (water adsorption, g H_2O/100 g adsorbent). There is only a 0.01 % likelihood that an *F*-value of this magnitude could arise due to random variation. A *p*-value below 0.0500 indicates that the corresponding model term is significant. Accordingly, *A*, *B*, *AB*, A^2, B^2 and C^2 are well agreed, whereas terms with *p*-values above 0.1000 are considered insignificant. The lack of fit *F*-value of 4.38 suggests there is a 9.39 % chance that such a high lack of fit *F*-value could be due to noise.

Similarly, the model *F*-value of 211.80 signifies that the model is significant for Response 2 (*CEC*). Again, there is only 0.01 % probability that such an *F*-value could be noise-driven. Terms with *p*-values below 0.0500 are deemed significant, namely *A*, *B*, *C*, A^2, B^2 and C^2 in this case. Terms with *p*-values above 0.1000 are

deemed insignificant. The lack of fit *F*-value of 3.86 implies that the lack of fit is not significant relative to pure error, with an 11.23 % likelihood that this *F*-value could result from noise.

Based on these experiments (Table VI), the lowest water adsorption was 25.45 g H_2O/100 g adsorbent and the highest was 29.09 g H_2O/100 g adsorbent. Meanwhile, the *CEC* varied from a minimum of 142.25 mg $CaCO_3$ g^{-1} to a maximum of 192.43 mg $CaCO_3$ g^{-1}.

TABLE VI. Statistical analysis for responses (water adsorbed amounts and C*EC* value)

Variable	Std. Dev.	Low	High
A: NaOH (mol/L)	0	2	3
B: Temperature, °C	0	60	90
C: *S*/*L* ratio, %	0	20	30
Water absorbed, g H_2O/100 g adsorbent	0.14	25.475	29.09*
CEC / mg $CaCO_3$ g^{-1}	1.42	142.35	192.43

Effect of variables on water adsorbed amounts and CEC *value*

To more thoroughly explore how synthesis parameters affect the adsorption properties of LTA-type zeolite, three-dimensional (3D) response surface plots were generated (Fig. 5). These plots demonstrate how NaOH concentration (*A*), temperature (*B*) and solid-to-liquid ratio (*C*) collectively influence both water adsorption capacity and cation exchange capacity.

The first row of Fig. 5 demonstrates the effects of process parameters on water adsorption (g H_2O/100 g adsorbent). NaOH concentration and temperature significantly influence water adsorption, whereas the solid-to-liquid ratio has a minor impact. Water adsorption increases with NaOH concentration up to around 2.5 M, then declines, reflecting the optimal concentration suggested by the negative quadratic coefficient ($-1.36A^2$). Temperature positively influences water adsorption ($+0.9189B$) initially, but diminishes at higher levels. The minimal effect of solid-to-liquid ratio is indicated by its small linear coefficient ($-0.1258C$).

The second row of Fig. 5 shows the response surfaces for cation-exchange capacity (*CEC*). Increasing NaOH concentration greatly enhances *CEC* ($+16.00A$), but overly high concentrations negatively affect it ($-13.85A^2$), possibly due to structural degradation. Temperature similarly shows a positive effect initially ($+8.04B$), slightly decreasing at higher temperatures ($-0.9220B^2$). The solid-to-liquid ratio has the smallest effect ($-1.38C$), indicating minimal influence on *CEC*. Overall, the response surface models underscore the need to optimize NaOH concentration and temperature to maximize both water adsorption and *CEC* while minimizing adverse structural alterations. Although the solid-to-liquid ratio does play a part, its effect is comparatively small. XRD results indicate that an excessively high solid loading (30 %) can impede nucleation, leaving quartz as the dominant phase (Run 3). The highest *CEC* (192.43 mg $CaCO_3$ g^{-1}) was achieved at 3

M NaOH, 90 °C and 25 % solid-to-liquid ratio, whereas the maximum water adsorption (29.09 g H_2O/100 g adsorbent) occurred at 2.5 M NaOH, 75 °C and 25 % solid-to-liquid ratio. XRD analyses confirmed that these conditions favor an LTA-type zeolite phase, with the best crystallinity obtained at 3 M NaOH, 90 °C (Run 17), consistent with its elevated *CEC* value. A balanced set of conditions that simultaneously account for both properties emerge at 2.5 M NaOH, 75 °C and 25 % *S*/*L* ratio (Run 7–11), although 3 M NaOH and 90 °C (Run 17) remains the best choice if maximizing *CEC* is the primary goal. Furthermore, to identify optimal synthesis conditions, XRD analysis was performed. As shown in Table VII and Fig. 6, all samples obtained through the statistical design exhibited the LTA-type zeolite phase. Fig. 6 highlights the distinctive reflections of LTA-type zeolite, confirmed by matching peaks to the 73-2340 Zeolite LTA standard in the Inorganic Crystal Structure Database (ICSD).

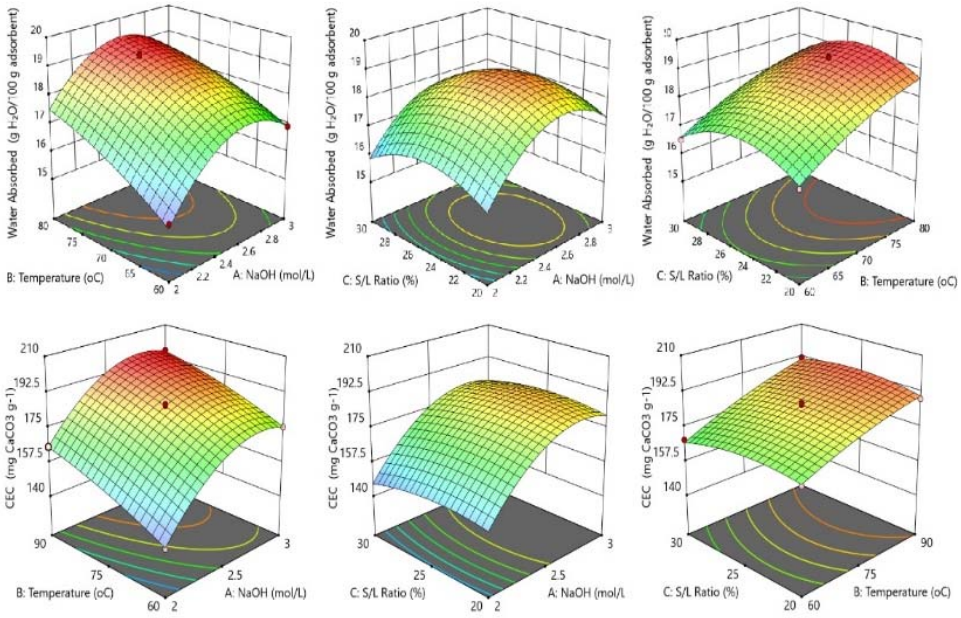

Fig. 5. Results of effecting variables on water adsorbed amounts and CEC value of LTA type zeolite.

Pawley refined X-ray patterns (Fig. 6, Table VII) confirm the synthesis window anticipated by the response surface model. At 2 M NaOH (Runs 1, 5, 6, 14) quartz dominates (63–78 %) and LTA remains below the 3 % detection limit, accompanied by 22–32 % amorphous aluminosilicate. Such behavior is characteristic of the dissolution reprecipitation constraint observed when alkalinity was inadequate for complete framework reconstruction.[36] Increasing the alkalinity to 2.5 M establishes a crystallization threshold even at 60 °C: Runs 2 and 3 contain 44

TABLE VII. XRD Results for of synthesized zeolite LTA

Run	Factor 1	Factor 2	Factor 3	LTA type zeolite	Quartz	Sodalite	Amorphous
	A: NaOH (mol/L)	*B*: Temp., °C	*C*: *S*/*L* / %	%	%	%	%
1	2	60	25	<3	78	–	22
2	2.5	60	20	44	38	4	6
3	2.5	60	30	52	23	4	21
4	3	60	25	62	28	5	5
5	2	75	20	<3	64	2	30
6	2	75	30	<3	65	3	32
7–11	2.5	75	25	70	20	4–6	2–4
12	3	75	20	75	15	3–5	5–7
13	3	75	30	77	13	2–6	6–8
14	2	90	25	11	63	3	23
15	2.5	90	20	65	31	0–3	3–8
16	2.5	90	30	68	25	0–3	3–8
17	3	90	25	95–97	2–3	–	<1

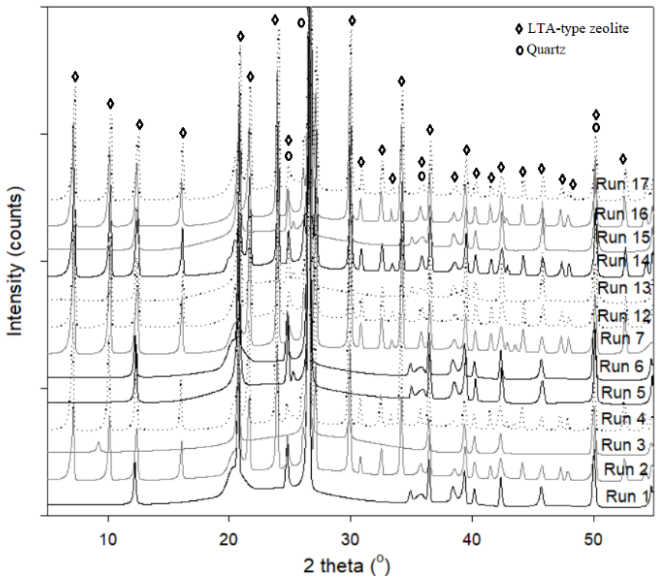

Fig. 6. XRD Results of diffractograms of the samples.

and 52 % LTA, respectively. The higher solid loading in Run 3 (30 % *S*/*L*) still leaves 21 % amorphous phase, illustrating the inhibitory effect of excessive slurry density on a ion mobility and nucleation.[39] With a concomitant rise in temperature to ≥ 75 °C, LTA crystallinity improves markedly. At 2.5 M NaOH and 75 °C (Runs 7–11), the products consistently contain approximately 70 % LTA, with quartz around 20 %, sodalite 4–6 % and only 2–4 % amorphous phase. The identical synthesis conditions applied to these runs resulted in similar phase compositions, as

summarized collectively in Table VII. The elevated water adsorption capacities observed in Runs 7–11 directly correlate with the high LTA content formed under these conditions. The highly porous LTA framework accounts for the enhanced water adsorption, while simultaneously elevated *CEC* values further confirm the dominant formation of the ion-exchangeable LTA zeolite phase. For Run 12 (3 M NaOH, 75 °C, 20 % *S*/*L*), the phase composition was estimated based on its similarity to neighboring runs, yielding approximately 75 % LTA, ~15 % quartz, 3–5 % sodalite, and 5–7 % amorphous content while at 3 M NaOH (Run 13) it reaches 77 % LTA with only 6–8 % amorphous residue. These observations mirror the positive interaction between the linear *A* (NaOH) and *B* (temperature) terms in the RSM surfaces. The optimum domain lies at high alkalinity and high temperature: Runs 15 and 16 (2.5 M NaOH, 90 °C) contain 65–68 % LTA with ≤8 % amorphous phase, whereas Run 17 (3 M NaOH, 90 °C, 25 % *S*/*L*) attains 95–97 % LTA (a = = 24.6127 Å, *Rwp* = 9.2 %) with only trace quartz and anatase. A residual line at $2\theta \approx 20.5°$ ($d \approx 4.33$ Å) detected in partially crystallized samples corresponds to sodalite and indicates an intermediate stage in route to LTA formation 25. Collectively, these phase assemblages corroborate the statistical model: high alkalinity (≥ 2.5 M) and elevated temperature (≥ 75 °C) are indispensable for phase-pure LTA, whereas lower NaOH or excessive solids loading suppresses nucleation, yielding quartz-rich or mixed products with diminished cation-exchange and water adsorption capacities.

Morphological and FTIR characterization results of best synthesis zeolite LTA (Run 17)

The scanning electron images show that the morphology of Run 17 sample was predominantly of cubic particles which are characteristic of LTA zeolite. High-magnification SEM images showed the presence of intergrown particles on the surface of cubes or between the cubes. The area marked with a black square in Fig. 7 was scanned by EDX. The EDX spectrum of sample Run 17 indicates that the main chemical elements present are Na, Al and Si, which are consistent with the chemical composition of LTA zeolite framework. The formation of the LTA structure was confirmed by the characteristic diffraction pattern observed in the XRD analysis.

High-magnification SEM images of Run 17 display well-defined cubic crystals ranging from sub-micron sizes up to approximately 2 μm, with sharp {100} faces and 90° edges, which is a morphology characteristic of low-silica zeolite LTA.[39] EDX analysis of the area highlighted in Fig. 7 yields an atomic ratio of Na ≈ Al ≈ Si, consistent with the ideal LTA framework composition ($Na_{12}[Al_{12}Si_{12}O_{48}]$). While cubic habit alone is not conclusive, the combination of this morphology, the stoichiometric Na–Al–Si balance, and the phase-pure LTA

reflections in the Pawley-refined XRD pattern (Fig. 6) collectively confirm that the product is LTA-type zeolite.

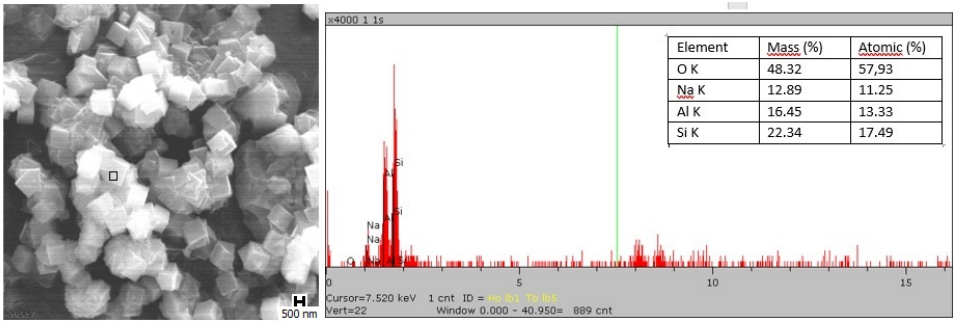

Fig. 7. SEM Results of Run 17 samples.

FTIR spectra were recorded from 4000 to 500 cm^{-1} using an FT-IR spectrometer and the KBr pellet technique. The FTIR spectrum of the sample synthesized under Run 17 conditions, which is the average yield of the synthesized zeolite LTA under optimal conditions (Run 17) was approximately 72±3 wt. %, is shown in Fig. 8. It was compared the calcined kaolinite (MK). In the metakaolin sample, a broad band at 793.10 cm^{-1} corresponds to Al–O bonds in Al_2O_3, while a vibration band at 1077.95 cm^{-1} is assigned to the Si–O stretch of SiO_2. Although the spectrum for Run 17 shows overall similarity to that of commercial-grade LTA zeolite, a distinct additional band at 638 cm^{-1} is observed, which is absent in the commercial sample. Specifically, peaks at 546, 667 and 1007 cm^{-1} represent T–O

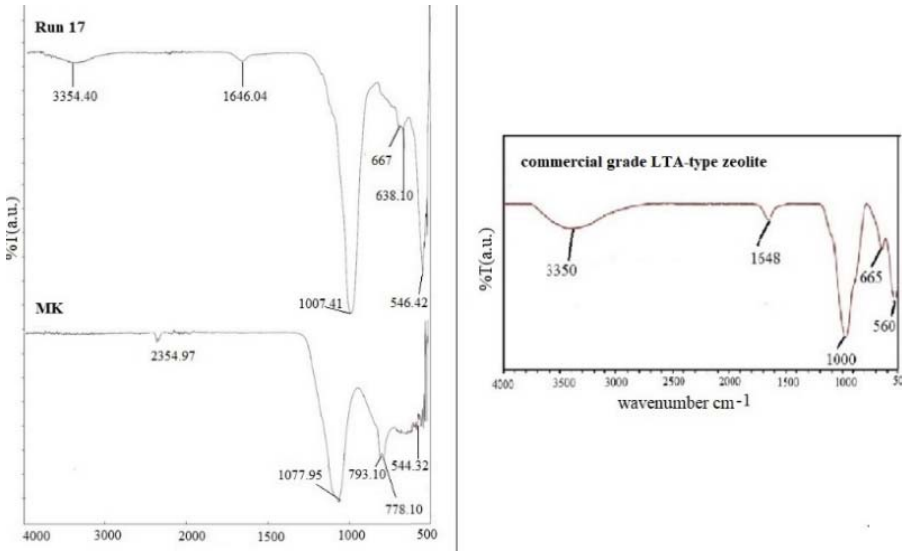

Fig 8. FTIR Results of Run 17 samples.

bending, double-loop bending, and TO_4 asymmetric stretching, respectively (T = Si or Al). Additionally, bands between 3000 and 3600 cm^{-1}, as well as at 1646.04 cm^{-1}, indicate intermolecular hydrogen bonding and interstitial water. These observations are consistent with earlier reports,[29,40] confirming the successful synthesis of LTA-type zeolite from MK under the selected optimal conditions. Moreover, the presence of strong absorption bands near 550–600 cm^{-1} and around 1000 cm^{-1} is widely recognized in the literature as indicative of a zeolite framework, reflecting the characteristic ring and tetrahedral vibrations of LTA-type structures. The obtained spectrum shows very good agreement with the reference FT-IR profile of commercial LTA-type zeolite (Fig. 8), while minor differences such as the 638 cm^{-1} band may reflect structural variations specific to the synthesized sample. Such shifts in vibrational modes from calcined kaolinite to the synthesized product highlight the reorganization of the aluminosilicate network, which is a key hallmark of the hydrothermal transformation into LTA zeolite.[40]

CONCLUSION

Low-silica zeolite LTA was successfully synthesized in high yield from Balıkesir-region kaolin via a two-step process combining metakaolinization at 800 °C and hydrothermal crystallization under alkaline conditions. Box–Behnken design and response-surface methodology (RSM) identified NaOH concentration and temperature as key factors controlling both cation-exchange capacity (*CEC*) and water adsorption, while excessive solid-to-liquid ratio inhibited nucleation. Crystallization toward the LTA framework occurred only above 2.5 M NaOH and 75 °C, with lower alkalinity or high slurry loading yielding quartz-rich or mixed phases. The optimal condition at 3 M NaOH, 90 °C and 25 % *S*/*L* produced nearly phase-pure LTA (≈97 %) with lattice parameter a = 24.6127 Å and *CEC* of 192 mg $CaCO_3$ g^{-1}. Water adsorption peaked at slightly milder conditions (2.5 M NaOH, 75 °C, 25% *S*/*L*), reflecting the narrow overlapping maxima predicted for both responses. XRD, SEM-EDX and FT-IR results demonstrated that the synthesized product exhibits cubic morphology and vibrational features consistent with LTA-type zeolite, closely resembling commercial materials. These results demonstrate that locally sourced kaolin can be converted into high-performance LTA zeolite without organic templates and under mild conditions, highlighting its potential as a cost-effective adsorbent or ion-exchange material for environmental applications.

ИЗВОД

СИНТЕЗА ЗЕОЛИТА LTA ИЗ КАОЛИНА И ЊЕГОВЕ ПЕРФОРМАНСЕ CBC И WAC МОДЕЛА: ОПИМИЗОВАНО ЦЕНТРАЛНИМ КОМПОЗИТНИМ ДИЗАЈНОМ

GÜL AKAR ŞEN

Dokuz Eylul University, Faculty of Engineering, Mining Engineering Department, İzmir, Turkiye

У овом раду представљен је исплатив начин синтезе зеолита LTA-типа из каолина који потиче из региона Balıkesir. Каолин је калцинисан на 800 °C да би се добио мета-каолин, који је затим третиран хидротермално у присуству NaOH при оптимизованим условима одређеним Box–Behnken експерименталним дизајном. Процесне променљиве концентрација NaOH, температура и однос чврсто/течно су систематски испитиване да се максимизира капацитет адсорпције воде и капацитет јонске измене (*CEC*). Модели квадратне регресије и ANOVA су потврдили да концентрација NaOH и температура имају најзначајнији утицај на формирање и перформансе зеолита. Карактеризација XRD, SEM и FTIR спектроскопијом потврдила је да се производ синтетисан при оптимални условима претежно састоји од зеолитских кристала LTA-типа, што је потврђено карактеристичним рефлексијама, морфологијом и вибрационим тракама. Узорак који је имао најбоље перформансе је имао *CEC* до 192 mg $CaCO_3$ g^{-1} и адсорпциони капацитет за воду до скоро 29 g H_2O по 100 g адсорбента. Ови резултати истичу потенцијал локално узоркованог каолина за производњу веома вредног зеолита, нудећи одрживу алтернативу увозним сировинама.

(Примљено 10. марта, ревидирано 8. априла, прихваћено 22. јула 2025)

REFERENCES

1. C. Ronco, R. Bellomo, *Crit. Care* **26** (2022) 135 (https://doi.org/10.1186/s13054-022-04009-w)
2. S. Chatterjee, T. Chatterjee, SH. Woo, *Chem. Eng. J.* **166** (2011) 168 (https://doi.org/10.1016/j.cej.2010.10.047)
3. M. Popaliya, A. Mishra, *Inter. J. Environ. Sci. Technol.* **20** (2023) 12919 (https://doi.org/10.1007/s13762-022-04603-z)
4. E. M. Flanigen, J. A. Rabo, *Micropor. Mesopor. Mater.* **47** (2001) 119 (https://doi.org/10.1016/S1387-1811(01)00301-8)
5. J. B. Adeoye, J. A. Omoleye, M. E. Ojewumi, R. Babalola, *Inter. J. Appl. Eng. Res.* **12** (2017) 755 (https://www.ripublication.com/ijaer17/ijaerv12n5_27.pdf)
6. E. Victor, I. P. Okechukwu, C. N. Uchenna, *GSJ* **10** (2022) 1913 (http://www.globalscientificjournal.com/researchpaper/HYDROTHERMAL_SYNTHESIS_OF_ZEOLITE_Y_FROM_OKPELLA_KAOLIN_CLAY.pdf)
7. V. Verdoliva, M. Saviano, S. De Luca, *Catalysts* **9** (2019) 248 (https://doi.org/10.3390/catal9030248)
8. N. Yu. Ul'yanovaa, E. Yu. Brazovskayaa, O. Yu. Golubevaa, O. V. Shamovab, *Petroleum Chem.* **63** (2023) 790 (https://doi.org/10.1134/S096554412305002X)
9. C. Algieri, E. Drioli, *Sep. Pur. Tchnol* **278** (2022) 119295 (https://doi.org/10.1016/j.seppur.2021.119295)
10. P. Bai, M. Y. Jeon, L. Ren, C. Knight, M. W. Deem, M. Tsapatsis, J. I. Siepmann, *Nat. Commun*. **6** (2015) 5912 (https://doi.org/10.1038/ncomms6912)
11. H. N. Tran, P. V. Viet, H. Chao, *Environ. Saf.* **147** (2018) 55 (https://doi.org/10.1016/j.ecoenv.2017.08.027)

12. P. Frontera, S. Candamano, A. Macario, F. Crea, L. A. Scarpino, P. L. Antonucci, *Mater. Lett.* **104** (2013) 72 (https://doi.org/10.1016/j.matlet.2013.03.138)
13. H. Zhang, A. Li, W. Zhang, C. Shuang, *J. Colloid Interface Sci.* **468** (2015) 128 (https://doi.org/10.1016/j.jcis.2015.10.006)
14. A. Ates, G. Akgül, *Pow Tech.* **287** (2016) 285 (https://doi.org/10.1016/j.powtec.2015.10.021)
15. A. A. Ahmed, Z. H. Yamani, *Mater. Chem. Phys.* **259** (2021) 124181 (https://doi.org/10.1016/j.matchemphys.2020.124181)
16. C. Baerlocher, L.B. McCusker, *Database of Zeolite Structures*, 2025, http://www.iza-structure.org/databases/ (accessed on 24 April 2025)
17. T. Ohgushi, S. Komarneni, A. S. Bhalla, *J. Porous Mater.* **8** (2001) 23 (https://doi.org/10.1023/A:1026518200875)
18. W. Wang, Q. Feng, K. Liu, G. Zhang, J. Liu, Y. Huang, *Solid State Sci.* **39** (2015) 52 (https://doi.org/10.1016/j.solidstatesciences.2014.11.012)
19. X. Shen, G. Qiu, C. Yue, M. Guo, M. Zhang, *Environ. Sci. Pollut. Res. Int.* **24** (2017) 21829 (https://doi.org/10.1007/s11356-017-9824-5)
20. M. K. Seliem, S. Komarneni, *Micropor. Mesopor. Mater* **228** (2016) 266 (https://doi.org/10.1016/j.micromeso.2016.04.010)
21. K.S Hui, C. Y. H. Chao, *Micropor. Mesopor. Mater* **88** (2006) 145 (https://doi.org/10.1016/j.micromeso.2005.09.005)
22. W. J. Roth, P. Nachtigall, R. E. Morris, J. Cejka. *Chem. Rev.* **114** (2014) 4807 (https://doi.org/10.1021/cr400600f)
23. A. E. Gaidoumi, A. C. Benabdallah, B. E. Bali, A. Kherbeche, *Arab. J. Sci. Eng.* **43** (2017) 191-197 (https://doi.org/10.1007/s13369-017-2768-8)
24. Hartati, D. Prasetyoko, M. Santoso, I. Qoniah,. W. L Leaw, P. B. D. Firda, H. Nur. *J. Chin. Chem. Soc.* **67** (2020) 911 (https://doi.org/10.1002/jccs.201900047)
25. I. Bojaddayni, M. E. Küçük, Y. Ouardi, I. Jilal, S. Barkany, K. Moradi, E. Repo, K. Laatikainen, A. A. Ouammou, *Min. Eng.* **198** (2023) 108086 (https://doi.org/10.1016/j.mineng.2023.108086)
26. T. B. H. Nguyen, H. T. Van*, Technol. Agron.* **4** (2024) e002 (https://doi.org/10.48130/tia-0023-0021)
27. M. Senila, O. Cadar, *Heliyon* **10** (2024) 25303 (https://doi.org/10.1016/j.heliyon.2024.e25303)
28. M. Gougazeh, *J. Taibah Univ. Sci.* **12** (2018) 247 (https://doi.org/10.1080/16583655.2018.1465714)
29. Y. Cui, Y. Zheng, W. Wang, *Minerals* **8** (2018) 338 (https://doi.org/10.3390/min8080338)
30. M. A. V Villaquirán-Caicedo, R. M. De Gutiérrez, M. Gordillo, N. C. Gallego, *Clays Clay Miner.* **64** (2016) 75 (https://doi.org/10.1346/CCMN.2016.0640201)
31. L. Ayele, J. Pérez-Pariente, Y. Chebude, I. Díaz, *Micropor. Mesopor. Mater.* **215** (2015) 29 (https://doi.org/10.1016/j.micromeso.2015.05.022)
32. L. Ayele, J. Pérez-Pariente, Y. Chebude, I. Diaz, *New J. Chem.* **40** (2016) 3440 (https://doi.org/10.1039/c5nj03097h)
33. S. K. Kirdeciler, B. Akata, *Adv. Powder Tech.* **31** (2020) 4336 (https://doi.org/10.1016/j.apt.2020.09.012)
34. B. Ait-Amir, P. Pougnet, A. El-Hami, *Embedded Mechatronic Sys. 2nd Ed*. ***2*** (2020) (ISBN: 9781785481901, eBook ISBN: 9780081019566)

35. M. R. Wang, D. C. Jia, P. G. He, Y. Zhou, *Mater. Lett.* **64** (2010) 2551 (https://doi.org/10.1016/j.matlet.2010.08.007)
36. C. Belviso, F. Cavalcante, A. Lettino, S. Fiore, *Appl Clay Sci.* **80**–**81** (2013) 162 (https://doi.org/10.1016/j.clay.2013.02.003)
37. B. B. Sousa, J. A. R. Rego, D. S. B. Brasil, M. C. Martelli, *Cerâmica* **66** (2020) 404 (https://doi.org/10.1590/0366-69132020663802758)
38. B. Fabbri, S. Gualtieri, C. Leonardi, *Appl. Clay Sci.* **73** (2013) 2 (https://doi.org/10.1016/j.clay.2012.09.019)
39. C. S. Cundy , P. A. Cox , *Micropor. Mesopor. Mater.* **82** (2005) 1 (https://doi.org/10.1016/j.micromeso.2005.02.016)
40. M. Alkan, Ç. Hopa, Z. Yilmaz, H. Güler, *Micropor. Mesopor. Mater.* **86** (2005) 176 (https://doi.org/10.1016/j.micromeso.2005.07.008).